J|A|C|S
ARTICLES
Published on Web 09/09/2003

Determination of Initial and Long-Term Microstructure Changes in Ultrahigh Molecular Weight Polyethylene Induced by Drawing Neat and Pyrenyl Modified Films

Chuping Luo,[†] Teresa D. Z. Atvars,[‡] Pavla Meakin,[§] Anita J. Hill,[§,||] and Richard G. Weiss*,[†]

Contribution from the Department of Chemistry, Georgetown University, Washington, D.C. 20057-1227, Departamento de Físico-Química, Instituto de Química, Universidade Estadual de Campinas, Caixa Postal 6154, 13084-971, Campinas, SP, Brazil, CSIRO Manufacturing and Infrastructure Technology, Private Bag 33 Clayton South MDC, Victoria 3169, Australia, and Department of Chemistry, Monash University, Clayton Victoria 3800, Australia

Received May 19, 2003; E-mail: weissr@georgetown.edu

Abstract: Deformation processes in gel-crystallized ultrahigh molecular weight polyethylene (**UHMWPE**) films with draw ratios (DR) as high as 96 have been investigated by X-ray diffraction (XRD), differential scanning calorimetry (DSC), and positron annihilation lifetime spectroscopy (PALS). In addition, low concentrations of pyrene molecules have been introduced at the time of film preparation from the gels or afterward by sorption after film preparation, and the polarization of their electronic absorption and fluorescence spectra at different draw ratios has been measured over a large temperature range extending to below the glass transition. The pyrene-doped films have been irradiated to introduce covalently attached 1-pyrenyl groups, and these films at two draw ratios have been employed to investigate over large temperature ranges (1) the steady-state fluorescence intensity and (2) the rates of diffusion of *N,N*-dimethylaniline (**DMA**). These data have been correlated with the XRD, DSC, and PALS information obtained on the unmodified films. On the basis of analyses of this body of information, a novel deformation model that explains the decreased crystallinity and increased mean free volumes in gel-crystallized **UHMWPE** at low draw ratios is proposed. It involves "stretch" and "flip" motions of microfibrils present in the undrawn films. The high crystallinity content and stiffer chains due to drawing **UHMWPE** films result in weak α- and β-relaxation processes, slower diffusion of **DMA** than in undrawn films, and orientation factors for doped pyrene molecules that are constant over a large temperature range. The overall picture that emerges allows several aspects of the morphology of **UHMWPE**, a polymer of fundamental importance in materials research, to be understood.

Introduction

Since the development of the Ziegler−Natta type catalysts,[1−3] various types of linear polyethylenes (**LPE**) have been manufactured. One of the most important **LPE**s from a commercial standpoint is ultrahigh molecular weight polyethylene (**UHMWPE**, $M_w > 10^6$).[4−6] Its low density, solubility properties, and high modulus and strength, especially in the form of drawn films and fibers,[7] have resulted in several important industrial applications, including the fabrication of surgical prostheses,[8] machine parts,[3] heavy-duty liners,[3,9] and boat sails.[9] Methods such as wide- and small-angle X-ray diffraction (WXRD and SXRD),[10−18] NMR spectroscopy,[5,13,19] FT-IR spectroscopy,[20]

[†] Georgetown University.
[‡] Universidade Estadual de Campinas.
[§] CSIRO Manufacturing and Infrastructure Technology.
[||] Monash University.

(1) Ziegler, K.; Holzkamp, E.; Breil, H.; Martin, H. *Angew. Chem.* **1955**, *67*, 541−547.
(2) Natta, G. *J. Polym. Sci.* **1960**, *48*, 219−239.
(3) Stevens, M. P. *Polymer Chemistry*; Oxford University Press: New York, 1999; Chapters 1 and 8.
(4) (a) Chanzy, H.; Day, A.; Marchessault, R. H. *Polymer* **1967**, *8*, 567−588. (b) Smith, P.; Chanzy, H. D.; Rotzinger, B. P. *Polym. Commun.* **1985**, *26*, 258−260. (c) Smith, P.; Chanzy, H. D.; Rotzinger, B. P. *J. Mater. Sci.* **1987**, *22*, 523−531.
(5) Rotzinger, B. P.; Chanzy, H. D.; Smith, P. *Polymer* **1989**, *30*, 1814−1819.
(6) Joo, Y. L.; Han, O. H.; Lee, H.-K.; Song, J. K. *Polymer* **2000**, *41*, 1355−1368.
(7) (a) Wang, L. H.; Ottani, S.; Porter, R. S. *Polymer* **1991**, *32*, 1776−1781. (b) Schellekens, R.; Bastiaansen, C. *J. Appl. Polym. Sci.* **1991**, *43*, 2311−2315.
(8) Marrs, H.; Barton, D. C.; Doyle, C.; Jones, R. A.; Lewis, E. L. V.; Ward, I. M.; Fisher, *J. J. Mater. Sci.: Mater. Med.* **2001**, *12*, 621−628.
(9) Chodak, I. *Prog. Polym. Sci.* **1998**, *23*, 1409−1442.
(10) (a) Aggarwal, S. L.; Tilley, G. P.; Sweeting, O. J. *J. Polym. Sci.* **1961**, *51*, 551−567. (b) Kiho, H.; Peterlin, A.; Geil, P. H. *J. Appl. Phys.* **1964**, *35*, 1599−1605.
(11) Seto, T.; Hara, T.; Tanaka, K. *Jpn. J. Appl. Phys.* **1968**, *7*, 31−42.
(12) (a) Van Aerle, N. A. J. M.; Braam, A. W. M. *J. Mater. Sci.* **1988**, *23*, 4429−4436. (b) Lemstra, P. J.; Van Aerle, N. A. J. M.; Bastiaansen, C. W. M. *Polym. J.* **1987**, *19*, 85−98.
(13) VanderHart, D. L.; Khoury, F. *Polymer* **1984**, *25*, 1589−1599.
(14) Russell, K. E.; Hunter, B. K.; Heyding, R. D. *Polymer* **1997**, *38*, 1409−1414.
(15) Hu, X. P.; Hsieh, Y. L. *Polym. J.* **1998**, *30*, 771−774.
(16) Bowden, P. B.; Young, R. J. *J. Mater. Sci.* **1974**, *9*, 2034−2051.
(17) Luo, C.; Guadala, N. A.; Price, J. L.; Chodak, I.; Zimerman, O. E.; Weiss, R. G. *Macromolecules* **2002**, *35*, 4690−4701.

polarized FT Raman spectroscopy,[21] transmission electron microscopy,[19,22,23] scanning electron microscopy,[24,25] atomic force microscopy,[26,27] and differential scanning calorimetry (DSC)[17,22,24] have been employed to explain the nature of the rather unique structure and texture of **UHMWPE** in its undrawn and drawn states and to unravel the mysteries of its intrinsically anisotropic properties.[13,15,17−27] In addition, we have probed the microstructure of undrawn and drawn **UHMWPE** by analyzing the photophysical properties of 1-pyrenyl groups covalently attached to polyethylene chains or of pyrene molecules doped into the films.[17] These results were compared to those from doped pyrene and covalently attached 1-pyrenyl groups in undrawn and drawn low- and high-density polyethylene (**LDPE** and **HDPE**) films.[28,29]

With increasing degrees of crystallinity and chain entanglement in **UHMWPE**, the storage modulus and the importance of α-relaxations (associated with large segmental motions of chains in the amorphous regions, but near crystallites[30]) increase, and the contribution from γ-relaxations (occurring along short chain segments in amorphous regions, but with important contributions from crystalline parts as well[30]) decreases.[18] Under ambient conditions, polyethylene fibrils exhibit mainly an orthorhombic crystalline structure,[10−17,31,32] and their X-ray diffraction patterns usually provide deflections from $(110)_o$ and $(200)_o$ lattices. In undrawn polyethylenes, the orthorhombic crystallites are usually distributed randomly. However, lamellae of **UHMWPE** are partially oriented, even in the undrawn state,[12a] and drawing increases the orientation of **UHMWPE** crystallites, as it does other polyethylenes.[17] The onset of crystallographic and morphological orientation occurs at lower compression ratios in **UHMWPE** than in **HDPE**, and greater resistance to deformation and more extensive strain recovery are also exhibited by **UHMWPE**. These differences in deformation behavior of **UHMWPE** and **HDPE** have been attributed to the larger number of tie molecules and higher degree of entanglement within the (limited) amorphous regions of **UHMWPE**.[33] A metastable monoclinic crystalline phase has been identified by WXRD when LPE is subjected to tension[17] or compression[11,14] beyond the yield point (i.e., where phase transformation and deformation processes occur).[10b,11]

The consequences of changes in the amorphous regions of polyethylenes must be known to understand (1) how nucleation and crystallization occur,[34] (2) what are the mechanisms by which guest molecules are oriented,[35,36] (3) how molecules diffuse[37,38] and permeate the polymer matrix,[39] and (4) how the local environment affects the dynamics of structural changes of guest molecules.[40] Several specific models have been advanced to explain the deformation processes of LPE.[12,41−43] A common feature of these models is large-scale, irreversible sliding and tilting motions of lamellae in the initial stages of drawing to form microfibrils.[44] These deformation processes are believed to occur in **LDPE** and **HDPE**,[41−43] as well as in **UHMWPE**.[12a,23]

In the present work, the properties of **UHMWPE** films with draw ratios (DR; i.e., the ratio of the lengths after and before drawing; see below) from 1 to 96 have been investigated by XRD, DSC, and PALS measurements. These data have been correlated with measurements of diffusion by *N*,*N*-dimethylaniline (**DMA**) in films based on the steady-state and dynamic fluorescence of covalently attached pyrenyl groups. Undrawn and drawn films modified with the lumophoric pyrenyl groups have been prepared by doping pyrene molecules into unmodified films either as their gels are dried (**UHMWPE-Py-g**, DR = 1, 9, and 48) or by diffusion after drying (**UHMWPE-Py-d**, DR = 1, 10), followed by irradiation and removal of the unattached pyrene molecules.[17] In addition, the temperature-dependent fluorescence of **UHMWPE-Py-g** films (DR = 1, 9, and 48) has been used to detect the onsets of chain relaxation processes and the polarized absorption, and emission of films doped with pyrene molecules (**UHMWPE/Py-g**, DR = 9 or **UHMWPE/Py-d**, DR = 10) has been measured between room temperature and −45 °C to determine how the guest molecules are oriented within the polymer matrix. These results demonstrate the stiffness of the microstructures of **UHMWPE**. They also indicate that the crystalline regions exert a significant influence on the properties of the amorphous parts of **UHMWPE**.

(18) Zamfirova, G.; Perena, J. M.; Benavente, R.; Perez, E.; Cerrada, M. L.; Nedkov, E. *Polym. J.* **2002**, *34*, 125−131.
(19) Uehara, H.; Matsuda, H.; Aoike, T.; Yamanobe, T.; Komoto, T. *Polymer* **2001**, *42*, 5893−5899.
(20) Sheiko, S.; Frey, H.; Möller, M. *Colloid Polym. Sci.* **1992**, *270*, 440−445.
(21) Bentley, P. A.; Hendra, P. J. *Spectrochim. Acta, Part A* **1995**, *51*, 2125−2131.
(22) Kunz, M.; Drechsler, M.; Möller, M. *Polymer* **1995**, *36*, 1331−1339.
(23) Sheiko, S. S.; Möller, M.; Kunz, M.; Deckmann, H. *Acta Polym.* **1996**, *47*, 492−497.
(24) Smith, P.; Lemstra, P. J. *J. Mater. Sci.* **1980**, *15*, 505−514.
(25) Smith, P.; Lemstra, P. J.; Pijpers, J. P. L.; Kiel, A. M. *Colloid Polym. Sci.* **1981**, *259*, 1070−1080.
(26) Sheiko, S. S.; Kunz, M.; Möller, M. *Vysokomol. Soedin.* **1993**, *35*, 1903−1912.
(27) Magonov, S. N.; Sheiko, S. S.; Deblieck, R. A. C.; Möller, M. *Macromolecules* **1993**, *26*, 1380−1386.
(28) (a) Naciri, J.; Weiss, R. G. *Macromolecules* **1989**, *22*, 3928−3936. (b) Brown, G. O.; Zimerman, O. E.; Weiss, R. G. *Polymer* **2002**, *43*, 6495−6503. (c) Brown, G. O.; Guardala, N. A.; Price, J. L.; Weiss, R. G. *J. Phys. Chem. B* **2002**, *106*, 3375−3382.
(29) (a) He, Z.; Hammond, G. S.; Weiss, R. G. *Macromolecules* **1992**, *25*, 1568−1575. (b) Jenkins, R. M.; Hammond, G. S.; Weiss, R. G. *J. Phys. Chem.* **1992**, *96*, 496−502. (c) Talhavini, M.; Atvars, T. D. Z.; Cui, C.; Weiss, R. G. *Polymer* **1996**, *37*, 4365−4374. (d) Zimerman, O. E.; Cui, C.; Wang, X.-C.; Atvars, T. D. Z.; Weiss, R. G. *Polymer* **1998**, *39*, 1177−1185. (e) Zimerman, O. E.; Weiss, R. G. *J. Phys. Chem. A* **1998**, *102*, 5364−5374. (f) Kósa, C.; Danko, M.; Fiedlerová, A.; Hrdlovic, P.; Borsig, E.; Weiss, R. G. *Macromolecules* **2001**, *34*, 2673−2681.
(30) (a) Boyd, R. H. *Polymer* **1985**, *26*, 323−347. (b) Boyd, R. H. *Polymer* **1985**, *26*, 1123−1133. (c) Talhavini, M.; Atvars, T. D. Z.; Schurr, O.; Weiss, R. G. *Polymer* **1998**, *39*, 3221−3232. (d) Jordens, K.; Wilkes, G. L.; Janzen, J.; Rohlfing, D. C.; Welch, M. B. *Polymer* **2000**, *41*, 7175−7192.
(31) Matthews, J. L.; Peiser, H. S.; Richards, R. B. *Acta Crystallogr.* **1949**, *2*, 85−90.
(32) Hermans, P. H.; Weidinger, A. *Makromol. Chem.* **1961**, *44−46*, 24−36.
(33) Boontongkong, Y.; Cohen, R. E.; Spector, M.; Bellare, A. *Polymer* **1998**, *39*, 6391−6400.
(34) Geli, P. H. *Polymer Single Crystals*; Wiley: New York, 1963.
(35) Michl, J.; Thulstrup, E. W. *Spectroscopy with Polarized Light*; VCH: New York, 1986.
(36) Phillips, P. J. *Chem. Rev.* **1990**, *90*, 425−436.
(37) Guillet, J. E. In *Photophysical and Photochemical Tools in Polymer Science*; Winnik, M. A., Ed.; D. Riedel: Dordrecht, 1986; p 467.
(38) (a) Saleem, M.; Asfour, A. F. A.; Dekee, D.; Harrison, B. *J. Appl. Polym. Sci.* **1989**, *37*, 617−625. (b) Schlotter, N. E.; Furlan, P. Y. *Polymer* **1992**, *33*, 3323−3342.
(39) Hill, A. J.; Weinhold, S.; Stack, G. M.; Tant, M. R. *Eur. Polymer J.* **1996**, *32*, 843−849.
(40) (a) Gu, W. Q.; Hill, A. J.; Wang, X. C.; Cui, C. X.; Weiss, R. G. *Macromolecules* **2000**, *33*, 7801−7811. (b) Ramesh, V.; Weiss, R. G. *Macromolecules* **1986**, *19*, 1486−1489. (c) Cui, C.; Naciri, J.; He, Z.; Jenkins, R. M.; Lu, L.; Ramesh, V.; Hammond, G. S.; Weiss, R. G. *Quim. Nova* **1993**, *16*, 578−585. (d) Cui, C.; Weiss, R. G. *J. Am. Chem. Soc.* **1993**, *115*, 9820−9821. (e) Tung, C.-H.; Yuan, Z.-Y.; Wu, L.-Z.; Weiss, R. G. *J. Org. Chem.* **1999**, *64*, 5156−5161. (f) Gu, W.; Warrier, M.; Ramamurthy, V.; Weiss, R. G. *J. Am. Chem. Soc.* **1999**, *121*, 9467−9468. (g) Gu, W.; Warrier, M.; Schoon, B.; Ramamurthy, V.; Weiss, R. G. *Langmuir* **2000**, *16*, 6977−6981. (h) Gu, W.; Weiss, R. G. *J. Org. Chem.* **2001**, *66*, 1775−1780.
(41) Kobayashi, K. In *Polymer Single Crystals*; Geli, P. H., Ed; Wiley: New York, 1963; p 473.
(42) Peterlin, A. *J. Polym. Sci., Part C* **1965**, *9*, 61−89.
(43) Peterlin, A. *J. Mater. Sci.* **1971**, *6*, 490−508.
(44) Wunderlich, B. *Macromolecular Physics*; Academic Press: New York, 1974; Vol. I.

On the basis of the XRD, DSC, and PALS data, a new deformation model for gel-crystallized **UHMWPE** is proposed in which the initial deformation involves "stretch" and "flip" motions of microfibrils that are present in undrawn films. These deformations are responsible for the initial decrease of crystallinity and increase in mean free volume of "holes" as **UHMWPE** is drawn (DR: 1 → 15). Deformations at draw ratios greater than 15 unfold the "stretched" and "flipped" microfibrils, allowing tighter packing of chains, increased crystallinity, and decreased sizes of "holes". More importantly, the total body of information presents a very comprehensive structural and dynamic picture at several length scales when **UHMWPE** is in different stressed states.

Experimental Section

Materials. Ultrahigh molecular weight polyethylene powder from DSM, Holland (Stamilan UH, $\overline{M_w} \approx 2.8 \times 10^6$), was used as received. Pyrene (Aldrich, 99%) was recrystallized from benzene, passed through an alumina column using benzene as eluant, and recrystallized twice from ethanol to yield mp 148.6−149.1 °C (lit mp 149−150 °C[45]). *N*,*N*-Dimethylaniline (**DMA**; Aldrich, 99%) was distilled, saturated with N_2, and stored in a refrigerator until it was used. Methanol (EM Science, HPLC grade), ethanol (EM Science, HPLC grade), xylenes (Baker, analyzed), and chloroform (Fisher, HPLC grade) were used as received.

Undoped and pyrene-doped **UHMWPE** films were prepared from the powder by an adaptation[17] of a previously described procedure.[12b] First, the powder was dissolved in hot xylenes or hot xylenes containing known concentrations of pyrene and was gelled. The gels were held in place on a sheet of aluminum foil to avoid shrinkage while they slowly dried in the air. Finally, the films were placed in a vacuum oven at room temperature for 6 h to remove residual xylenes. Films prepared in this fashion were not porous. Pyrenyl groups were attached (yielding **UHMWPE-Py-g**) by irradiation of a **UHMWPE/Py-g** film ([Py] = 2.8×10^{-3} mol kg^{-1}; based on the average film thickness, the optical density at several positions on the film surface, and the molar extinction coefficient of pyrene at 335 nm in hexane, 55 000 M^{-1} cm^{-1} [46]) in vacuo at >300 nm and subsequent removal of unattached pyrene molecules by immersing the film in refluxing chloroform for a total of 1 month to remove unattached pyrene and other aromatic molecules.[17,28b] The chloroform was replaced daily until no more pyrenyl-like molecules could be extracted. The film surfaces were then washed with methanol.[17] The concentration of attached 1-pyrenyl groups was too low to observe its characteristic absorption bands.

Instrumentation and Procedures. Unless indicated otherwise, experiments were carried out at room temperature. UV−vis absorption spectra were measured at three different positions on each film using a dual-beam Cary 300 Bio UV−visible spectrophotometer. To obtain linear dichroic absorption spectra, a pair of Glan-Nicol prism polarizers was inserted in the optical path of the reference and sample beams of the spectrophotometer. Films were mounted vertically with respect to their draw direction. While the films were kept stationary for the duration of each set of measurements, spectra were recorded with the electric vector of the polarized light parallel ($OD_{\parallel}$, vertical) and perpendicular ($OD_{\perp}$, horizontal) to the draw direction. Low-temperature measurements were performed by means of a homemade optical chamber in which the temperature can be adjusted precisely from room temperature to −50 °C. The temperature was read from a thermometer (±1 °C) that was inserted into the sample chamber. Spectra from three different parts of each film were ratioed individually and averaged.

X-ray diffraction (XRD) data were collected on a Rigaku RAPID/XRD image plate system with Cu Kα ($\lambda = 1.54056$ Å) X-rays from a Rigaku generator operated at 46 kV and 46 mA. Drawn or undrawn **UHMWPE** films were mounted vertically on the sample support. The positions of the films were set so that the X-ray beam was perpendicular to the film surface and the draw direction (A in Figure 1), parallel to the film surface but perpendicular to the draw direction (B in Figure 1), or parallel to the film surface and the draw direction (C in Figure 1). Films in the (B) and (C) positions were oriented first in the (A) position, making sure that the radial diffractions from the $(110)_o$ and $(200)_o$ planes of orthorhombic crystallites[17] were symmetric circles for undrawn films or on the equatorial (for B) or meridian (for C) lines for drawn films. The films were then rotated on one axis by 90° to attain positions (B) or (C). Degrees of crystallinity from XRD measurements were calculated as averages of values from three pieces of film that were rotated horizontally during data collection. Sample and background data sets were deconvoluted from 1° to 90° in 2θ in 0.020° steps and then analyzed using MDI (Jade version 5) software.[47]

Differential scanning calorimetry (DSC) was performed under a N_2 atmosphere on 4.0−5.5 mg film samples in closed aluminum pans using a TA 2910 DSC cell interfaced to a TA Thermal Analyst 3100 controller. The heating rate was 5 °C/min, and the cooling rate was uncontrolled and depended on the difference between the sample and ambient temperatures.

Fluorescence measurements at various temperatures were obtained using an instrument described previously.[48] Films were cooled to −233 °C under vacuum in the chamber of a cryostat and then warmed progressively to 127 or 137 °C while spectra were recorded at intervals of 10 °C. Finally, the samples were recooled to room temperature. The area under each fluorescence curve was integrated, and the emission spectra were deconvoluted using Grams/32 software[49] to obtain the relative area and the full peak-width at half-height (fwhm) of the emission peak at the blue-edge ($\lambda_{em} = 377$ nm); R was ≥ 0.999 in all cases. Other fluorescence and excitation spectra, including polarized ones, were measured using a Spex Fluorolog III spectrofluorimeter with a 150 W lamp. Excitation spectra are corrected for detector response.

For polarized fluorescence spectral measurements, a pair of Glan-Nicol prism polarizers was inserted in the excitation and emission optical path of the spectrofluorometer. Front-face emission and excitation spectra between room temperature and −45 °C were obtained by placing the films in a homemade thermostating device. The temperature was read from a thermometer (±1 °C) that was inserted into the sample chamber. Films were mounted vertically with respect to their draw direction, and their faces were perpendicular to the excitation beam; the angle between the excitation and emission optical paths was 22.5°. The spectra were recorded while the electric vector of the polarized excitation and emission beams were parallel or perpendicular to the drawing direction of the films. Results are based on polarized emission spectra of three different parts of each film that were ratioed individually and averaged.

Positron annihilation lifetime spectroscopy (PALS) measurements were performed using an automated EG&G Ortec fast-fast coincidence unit, temperature stabilized at 23 ± 1 °C. Two identical sample stacks, 1.5 mm thick, were placed on either side of a ^{22}Na source, and the sample-source sandwich was placed between the detectors. The timing resolution of the system was 275 ps based on a ^{60}Co source with energy windows set to ^{22}Na events. OrthoPositronium (**oPs**) pick-off annihilation characteristics (τ_3, I_3) were measured. Data points represent the average of at least five spectra for τ_3.

Procedure for Drawing UHMWPE Films. Strips of films were held at the edges by compression clamps and heated 2−4 mm over a hot plate (130−140 °C) while being lengthened in small increments. Thicker films allowed higher draw ratios. Initially, films were drawn

(45) Perrin, D. D.; Amarego, W. L. F. *Purification of Laboratory Chemicals*, 3rd ed.; Pergamon Press: New York, 1988; p 267.
(46) Perkampus, H.-H. *UV−Vis Atlas of Organic Compounds*, 2nd ed. (part 2); VCH: New York, 1992.
(47) MDI Jade 5 software for X-ray diffraction pattern processing from Materials Data, Inc., Livermore, CA.
(48) Atvars, T. D. Z.; Talhavini, M. *Quim. Nova* **1995**, *18*, 298−300.
(49) Grams/32 software from Galactic Industries Corp..

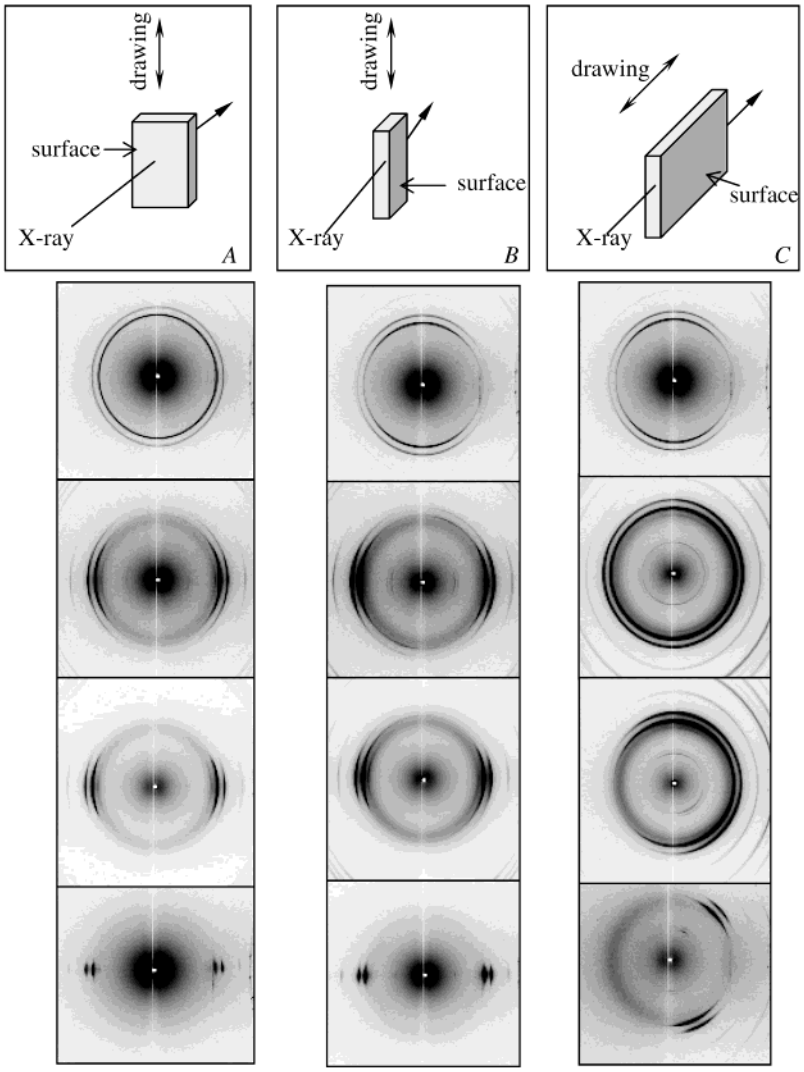

Figure 1. X-ray diffraction patterns of gel-crystallized **UHMWPE** films at (from top to bottom) DR = 1, 2, 4, and 78. The orientations for obtaining the diffraction patterns are shown at the top of each column.

to DR = 6−10. Pieces of this film were drawn further, and the process was repeated on pieces that were beyond the "neck" portions up to DR = 96.

Preparation and UV−Vis Irradiation of Pyrene-Doped (by Diffusion; UHMWPE/Py-d) DR = 1 and 10 UHMWPE Films. A piece of **UHMWPE** film was immersed in 0.05 M pyrene in a chloroform solution at 40 °C for 3 days. The film was rinsed with methanol three times to clean the surfaces and evacuated under ca. 0.5 Torr for 6 h. The drawn (DR = 10) and undrawn **UHMWPE/Py-d** films were flame-sealed in flattened Pyrex capillaries at $<10^{-5}$ Torr. Both were irradiated at >300 nm for 30 min on each face at a distance of ca. 5 cm from a Hanovia 450 W medium-pressure Hg arc. Following irradiations, they were extracted and washed[17] to yield 1-pyrenyl-attached films (**UHMWPE-Py-d**).

Diffusion of DMA between Methanol and DR = 1 and 10 UHMWPE-Py-d Films. A **UHMWPE-Py-d** film was placed in a flattened, closed quartz capillary that was immersed in a Pyrex cuvette filled with dodecane. The cuvette was placed in a thermostated cell holder in the spectrofluorimeter and maintained at 15−55 °C using a VWR 1140 circulating water bath. Temperature was measured with a thermistor that was in contact with the sample cuvette; readings were calibrated to temperatures of a thermometer directly in the dodecane liquid. For in-diffusion, fluorescence intensity measurements (λ_{em} 377 nm; λ_{ex} 343 nm) commenced immediately after an ca. 1.5 mL aliquot of a N_2-saturated 0.95 M **DMA**/MeOH solution, which had been equilibrated at the same temperature as the film, was decanted from a connected bulb into the capillary. Measurements were made at frequencies of 0.2 s for the first 30 min, 0.5 s for the second 30 min, and 1 s thereafter. Usually, more than 10 000 data points were collected, depending on the time needed to approach equilibrium. Out-diffusion measurements were made as above after removal of the **DMA** solution and replacement of it with 2.0 mL of temperature-equilibrated methanol. Each film was immobilized for the duration of each run; runs were repeated from two to four times at each temperature, and average values are reported.

Results and Discussion

X-ray Diffraction Studies. The XRD diffraction patterns of undrawn **UHMWPE** samples in the (A), (B), and (C) positions are quite different (Figure 1). Although diffractions from the (A) and (B) positions have been measured, diffraction from the (C) position has not. As will be shown, results from position (C) are important to analyses of the orientational and morphological changes that polymer chains suffer when films are drawn. The arcs in the diffraction patterns from the edges in (B) and (C) are centered on the meridian, suggesting that the polyethylene chains are already preferentially packed anisotropically.[12a] The symmetric, circular XRD pattern from the (A) position implies that the crystals are oriented randomly with respect to

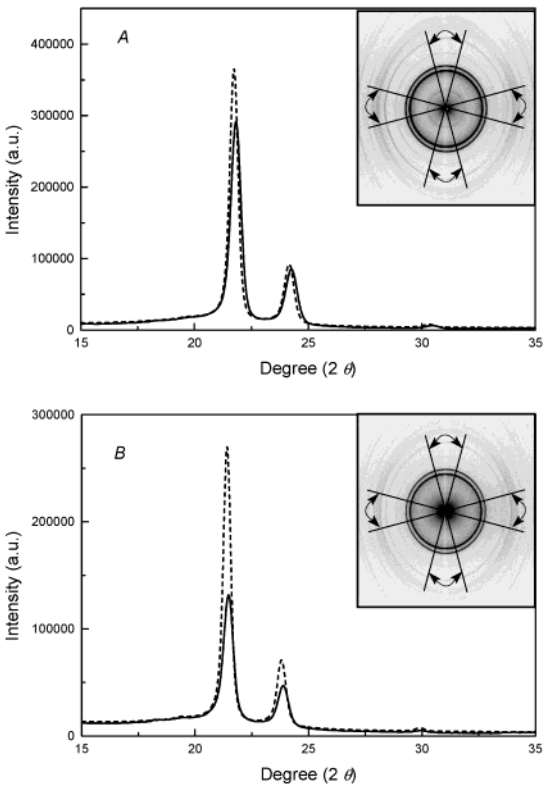

Figure 2. The insets are the radial XRD images, and the 30° arcs define the integration limits for the equatorial region (−) and meridian region (- - - -) diffractions of an undrawn **UHMWPE** film prepared from the gel without holding the edges in place; see text for details. Data for (A) and (B) were collected at positions defined by (A) and (B) in Figure 1.

an axis perpendicular to the major surface. In undrawn polyethylene, the crystals are orthorhombic with their *c*-axis parallel to the zigzag polyethylene chains.[14,17] Because the *c*-axis of an orthorhombic unit cell is perpendicular to the lamella surface,[50] it is also preferentially perpendicular to the major film surfaces (i.e., the lamellar surfaces are preferentially parallel to the major film surfaces).

This predrawing orientation may arise during film preparation. In their gel form,[12b] films are fixed to a surface so that they cannot shrink as their swelling solvent, xylene in our case, is removed slowly. The natural tendency of the films, to shrink along their lengths and breadths, is stopped; only their thickness can be reduced. In essence, the drying procedure is tantamount to "drawing". This is confirmed by the XRD patterns of an **UHMWPE** film that was dried without fixing the edges so that it could contract in all dimensions as the solvent evaporated (Figure 2). Unlike the XRD patterns of the undrawn film in Figure 1B, there is no significant difference between the image patterns from positions (A) and (B) for the sample that was allowed to contract (insets in Figure 2).

However, as can be seen from the plots of the diffraction intensities integrated over the two 30° equatorial and the two 30° meridian regions, the X-ray patterns of the unfixed sample are slightly different when viewed along the surface and edges (Figure 2). Although the intensities of the equatorial and the meridian regions at sample position (A) are quite similar, the corresponding intensities at sample position (B) are not. In the latter, the diffraction intensity of the meridian, especially, is much higher than that of the equatorial, suggesting that some crystallites orient preferentially with their *c*-axis perpendicular to the film surface even in a **UHMWPE** film dried with unfixed edges. Differences between the rates at which the xylene evaporates from the surfaces and edges may be responsible for the anisotropy observed here.

As a **UHMWPE** film was drawn to twice its length, the diffraction pattern in position (A) changed from being concentric rings (DR = 1) to arcs along the equatorial axis. Polyethylene chains were being displaced so that the *c*-axis of the orthorhombic unit cell now lies preferentially parallel to the major film surfaces (i.e., the lamellar surfaces were preferentially perpendicular to the film surfaces). Along position (B), a dramatic change of the preferred orientation of the *c*-axis of the orthorhombic unit cell is indicated by the movement of the arc from along the meridian (DR = 1) to the equatorial axis. At the same time, the pattern from position (C) changes from arcs (DR = 1) to concentric circles (i.e., from anisotropically oriented *c*-axes to randomly oriented ones)! According to currently favored models for polyethylene deformation, the initial stages of draw involve large-scale irreversible sliding, tilting, and phase changes of lamellae, resulting in the formation of microfibrils.[42,43] This model has also been applied to the deformation of gel-crystallized **UHMWPE**.[12a,23] Our data are incompatible with this explanation.

Nevertheless, it is clear that the XRD pattern of the undrawn film at position (A) is like that of the DR = 2 film at position (C) and the patterns of the undrawn film at positions (B) and (C) can be correlated with those of the DR = 2 film at positions (A) and (B). On the basis of these observations, we suggest a modification of the current deformation models at the initial deformation stages, at least as they apply to gel-crystallized **UHMWPE** (Figure 3). According to this model, microfibrils are present in undrawn **UHMWPE** films and are arranged somewhat anisotropically (Figure 3A). Although bundles of microfibrils that appear to be the initial stage of spherulitic structure formation have been observed on the surface of poly(4-methyl-1-pentene) films,[50] bundles of microfibrils in **UHMWPE** may remain together in sheaves packed perpendicular to the film surface (on average), and their ends may bend back into the film near the surfaces (Figure 3A). If this model is correct, only the bending ends of microfibrillar bundles can be detected near the major film surfaces.[26] This arrangement generates a set of XRD patterns for an undrawn **UHMWPE** in which the *c*-axis of an orthorhombic unit cell is preferentially perpendicular to the major film surface while the *a*- and *b*-axes are randomly arranged. As the film is drawn to DR = 2, the microfibrils are stretched without significant sliding of lamellae, so that the lamellae "flip" 90° (Figure 3B) and are isotropically distributed with respect to position (C).

Further drawing improves the degree of orientation of the polyethylene chains. As shown in Figure 1, the $(110)_o$ and $(200)_o$ diffractions become more and more condensed along the equatorial axis when the film is in positions (A) and (B) as the draw ratio is increased from 2 to 78. The sharp spots of the diffractions from the DR = 78 film in positions (A) and (B) indicate that most microfibrils are aligned along the drawing direction. The patterns viewed from position (C) also indicate that the chains become more oriented as the draw ratio increases,

(50) Sperling, L. H. *Introduction to Physical Polymer Science*, 3rd ed.; Wiley: New York, 2001; Chapter 6.

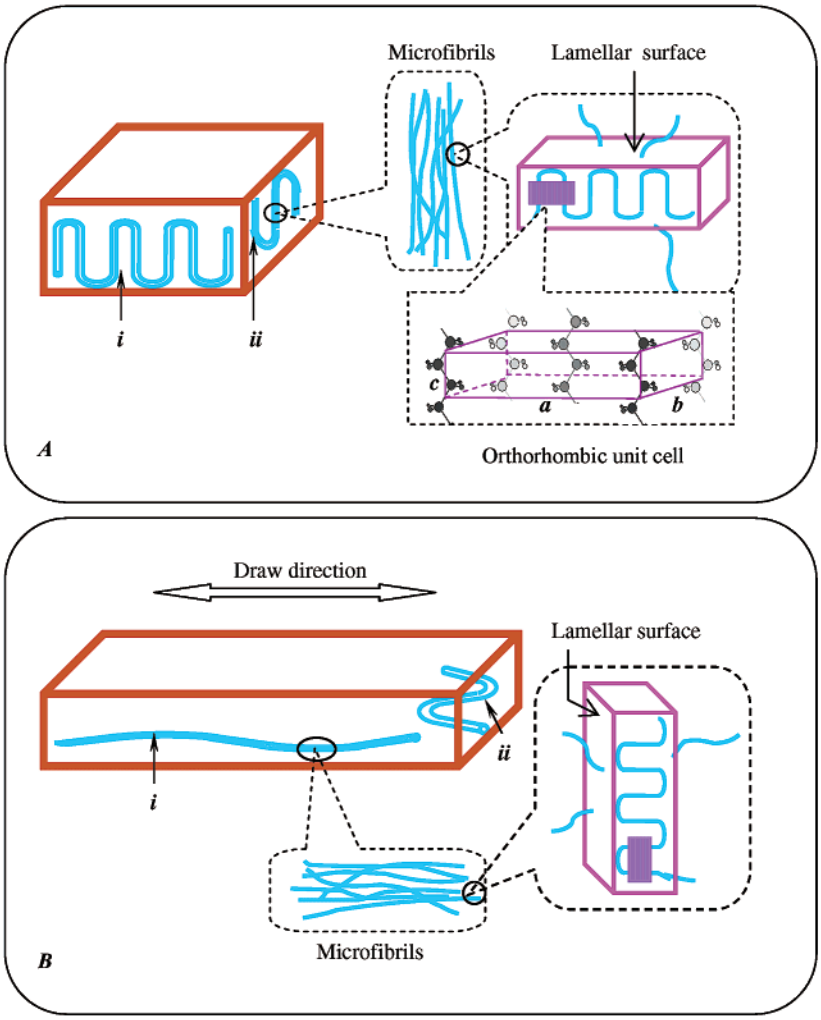

Figure 3. Cartoon representation of **UHMWPE** microstructures according to the deformation model for drawing from DR = 1 (A) to DR ≈ 2 (B). (i) and (ii) represent microfibrils along the drawing direction and perpendicular to it, respectively.

although the signals condense to a position along neither the meridian nor the equatorial axis. The observation of $(110)_o$ and $(200)_o$ may arise from the slightly tilting of $(110)_o$ and $(200)_o$ planes to the X-ray beam, which is coaxial to the drawing direction in position (C). XRD patterns of the DR = 78 film suggest that virtually all of the entanglements of polyethylene fibrils, especially screwlike ones,[27] have been removed.

Monoclinic crystals, whose main diffraction planes are $(001)_m$ ($2\theta = 19.5°$), $(200)_m$ ($2\theta = 23.1°$), and $(-200)_m$ ($2\theta = 25.1°$), are believed to be a minor component produced during the deformation of polyethylene. Three diffraction signals not present in the undrawn films (indicated by circles or arcs located closer to the origin than $(110)_o$ and $(200)_o$ in Figure 1) are evident at draw ratios from 2 to 78. The diffraction at $2\theta = 19.5°$, indicated by arrow-3 in Figure 4, is ascribed to the $(001)_m$ diffraction, and the peak at $2\theta = 11.8°$, indicated by arrow-2, is the $(100)_o$ diffraction.[11] However, the peak at $2\theta = 10.7°$, indicated by arrow-1, cannot be indexed as being from either a monoclinic or an orthorhombic crystal. It might be triclinic in origin,[51,52] arising from additional distortions of the orthorhombic crystalline form.

To explore the time-dependent morphological changes that attend drawing, the XRD pattern of **UHMWPE** films has also been collected 18 months after being drawn to DR = 9 and 96. The monoclinic diffraction of the freshly drawn DR = 9 film (Figure 5A-1) was no longer present in the aged sample (Figure 5A-2). However, no significant changes in the XRD of the DR = 96 film occurred after 18 months (Figure 5B). The lack of change in the more extended film implies that monoclinic crystals are less stable in low DR films than in high DR ones. The temporal morphological changes may be due to relaxation phenomena, possibly recrystallization processes, in **UHMWPE**.[9]

Film Crystallinities from DSC Thermograms and XRD. The crystallinities of the drawn films were calculated from both XRD and DSC data (Table 1). The DSC measurements are less precise because of the difficulty in locating accurately the area under the melting curves. They are based on the ratios between the heats of fusion of the **UHMWPE** samples and that of a single crystal of polyethylene, 286 J/g.[53] The XRD values were calculated from the ratio between the areas under crystal diffractions and the total area.[5,17,32,54] In the range $2 \leq DR < 15$, the calculated crystallinities are lower than that of the

(51) Frank, F. C.; Keller, A.; O'Connor, A. *Philos. Mag.* **1958**, *8*, 64−74.
(52) Hayashida, T. *J. Phys. Soc. Jpn.* **1962**, *17*, 306−315.
(53) Gray, A. P. *Thermochim. Acta* **1970**, *1*, 563−579.
(54) Challa, G.; Hermans, P. H.; Weidinger, A. *Makromol. Chem.* **1962**, *56*, 169−178 and references therein.

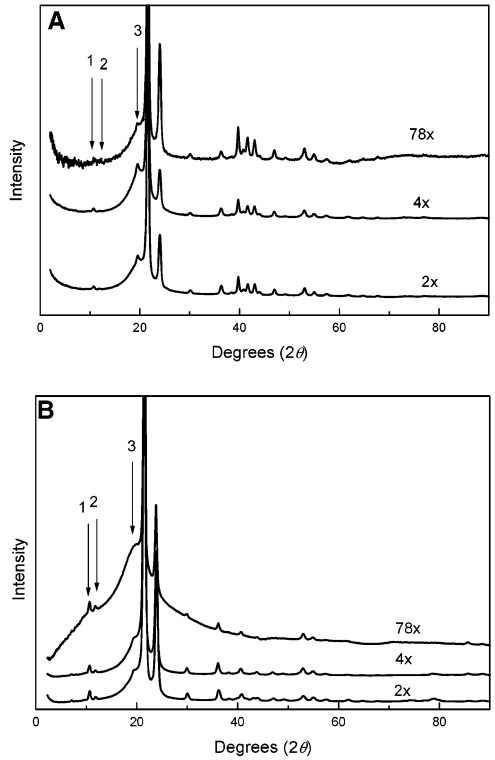

Figure 4. X-ray diffraction patterns of gel-crystallized **UHMWPE** with different draw ratios collected at setup-A (A) and setup-C (B) positions as defined in Figure 1. The curves are offset from each other on the vertical axis for clarity.

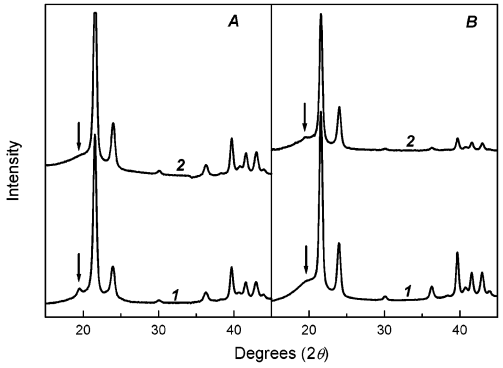

Figure 5. X-ray diffraction patterns of gel-crystallized **UHMWPE** films (setup-A position as defined in Figure 1) recorded immediately after (1) and 18 months after (2) drawing to DR = 9 (A) and DR = 96 (B).

undrawn film according to XRD measurements; when DR ≥ 32, crystallinities are higher than that of the undrawn film.

The initial decrease in crystallinity as **UHMWPE** is drawn ($2 \leq DR < 15$) suggests that tightly packed microfibrils become distorted as strain is applied to undrawn films. During the initial deformation stage (DR from 1 to 2), the "flip" of the microfibrils consists of a combination of chain motions (Figure 3B):

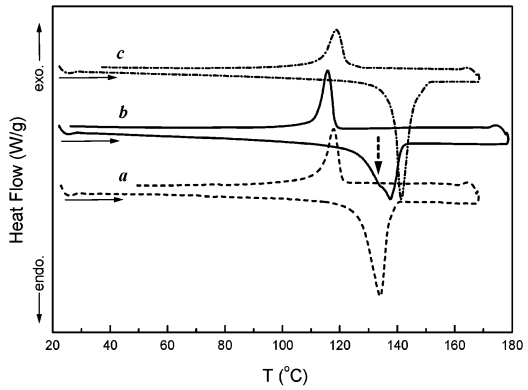

Figure 6. First heating (endotherms) and cooling (exotherms) DSC thermograms of undrawn (a), DR = 10 (b), and DR = 78 (c) **UHMWPE** films. The temperatures of maximum heat flow are 134 (a), 137 (b), and 141 °C (c). The horizontal arrows indicate the direction of temperature changes. See text for an explanation of the vertical arrow.

microfibrils oriented parallel to the drawing direction are "stretched" (i-arrangement in Figure 3); those oriented perpendicular "flip" by 90° (ii-arrangement in Figure 3); and those oriented between the two extremes may suffer a combination of both types of motions. Regardless of their type, the microfibril motions distort interchain packing in **UHMWPE** and decrease crystallinity. Because both the "stretch" and the "flip" motions reorient lamellae by ca. 90°, the initial loss of crystallinity is not accompanied by a decrease in fibril orientation (as measured crystallographically). At DR > 15, the microfibrils are forced to pack tightly again as they unfold,[12a] most ii-microfibrils are displaced or unfolded into the i-arrangement (Figure 3B), and the net crystallinity of **UHMWPE** increases. This model is consistent with scanning force microscopy images of drawn **UHMWPE** in which the surfaces formed by the displacement of microfibrils at DR = 10 are rougher than those at DR = 70.[23]

Despite the lack of precision in the crystallinity measurements from DSC, the thermograms do offer insights into the consequences of film drawing that are not available from XRD. For instance, thermograms of **UHMWPE** films with DR = 2−10 exhibit a shoulder endotherm prior to the temperature of maximum heat flow during the first heating scan (vertical arrow in Figure 6b). This feature was absent in the corresponding thermograms of undrawn and DR > 15 films (Figure 6a and c). The XRD patterns, as well as our previous studies,[17] indicate that the minor crystal components, especially for those that are monoclinic, are draw ratio dependent and increase in relative intensity up to DR = 15 and decrease thereafter. On that basis and the overall decreased crystallinity that occurs at low draw ratios, we attribute the shoulder endotherm to the melting of monoclinic or triclinic crystals. As expected, melting anneals and erases the memory of drawing-induced distortions; the first

Table 1. Crystallinities (%) of Drawn **UHMWPE** Films Calculated from XRD and DSC Data[17]

DR		1	2	4	10	15	32	52	78
XRD[a]	crystallinity	85 ± 3	72 ± 7	77 ± 6	82 ± 3	85 ± 4	90 ± 3	93 ± 2	94 ± 4
	$\Delta_{crystallinity}$[b]	0	−15 ± 9	−9 ± 8	−4 ± 5	0	6 ± 9	9 ± 4	11 ± 6
DSC[c]	crystallinity	95 ± 2	91 ± 4	80 ± 3	89 ± 2	93 ± 2	95 ± 2	94 ± 3	97 ± 2
	$\Delta_{crystallinity}$[b]	0	−4 ± 5	−16 ± 4	−6 ± 3	−2 ± 3	0	−1 ± 4	2 ± 3

[a] Average of measurements on three films rotated horizontally from −180 to +180° to average different orientational distributions. [b] $\Delta_{crystallinity} = 100 \times [crystallinity_{(drawn)} - crystallinity_{(undrawn)}]/crystallinity_{(undrawn)}$. [c] Average of heats from first heating thermograms on 4−6 films.

cooling and second heating thermograms of the drawn films are like those of the undrawn film.

The crystallinities of undrawn **UHMWPE-Py-g**, 82 ± 2% (XRD) or 89 ± 4% (DSC), and undrawn **UHMWPE-Py-d**, 84 ± 3% (XRD) or 90 ± 3% (DSC), are very close to that of undrawn **UHMWPE** (Table 1). On the basis of these results, we believe that the presence of pyrene molecules does not have a detectable influence on the morphology of the polymer chains, but it may affect local diffusivity and orientations (i.e., micromorphological properties; vide infra).

Free Volume in UHMWPE Films. The effects of draw ratio on the amorphous region of **UHMWPE** can be correlated with changes of the "hole" mean free volume. The free volume in polymers can be calculated from group contribution theory or molecular simulations.[55] However, theoretical models do not take into account the influence of the crystalline phase on the amorphous phase (and vice versa). A powerful tool to determine free volume in polymer films is positron annihilation lifetime spectroscopy (PALS).[56,57]

In the PALS technique, an orthoPositronium (**oPs**) becomes localized in "cavities" and measures the local free volume indirectly as a function of the electron density of the environment.[58] Cavities with less volume have higher local electron densities and shorter **oPs** lifetimes, τ_3.[59] The statistical weight of the **oPs** annihilation component, I_3 (note that there are usually two other decay components that are not related to pick-off annihilation), reflects the relative concentration of cavities in the volume of polymer probed and the positronium formation probability. The semiempirical models that allow calculation of the average size of the spherical[40a] or ellipsoidal[60] free volume elements from τ_3 are used usually for comparative, rather than quantitative, purposes. Interpretation of I_3 is complicated by its dependence on relative free volume element concentration and the probability of **oPs** formation. In polyethylene, contact time with the positron source reduces the formation probability over time by producing electron or positron scavengers. For this reason, characteristic I_3 values taken at early times during the measurement are used for comparison.[40a]

In the absence of special complications, the longest-lived decay from **oPs** pick-off annihilation, τ_3, can be related to a mean spherical cavity radius, R, by the semiempirical eq 1[61] in which the units of R are angstroms when the units of τ_3 are nanoseconds.

$$\tau_3 = \frac{1}{2}\left[1 - \frac{R}{R + 1.66} + \frac{1}{2\pi}\sin\frac{2\pi R}{R + 1.66}\right]^{-1} \qquad (1)$$

The subtleties of interpretation of PALS results in semicrystalline polymers and copolymers have been reviewed recently.[62]

Table 2. OrthoPositronium (**oPs**) Lifetimes and Intensities, and Calculated Mean Free Volumes (V_{PE}) Assuming Spherical Cavities in **UHMWPE** Films at Different Draw Ratios

DR	**oPs** lifetime τ_3 (±0.03 ns)	**oPs** intensity I_3 (%, ±0.5%)	V_{PE} (Å^3)	$\Delta(V_{PE})^a$ (%)
1	2.23	18.7	119.7	0
4	2.31	19.5	127.7	6.7
10	2.28	20.9	124.7	4.2
15	2.18	18.0	114.8	−4.1
32	2.12	20.5	109.0	−8.9
52	2.21	19.9	117.8	−1.6
78	2.12	18.5	109.0	−8.9

[a] Δ(free volume) = $\Delta(V_{PE}) = 100[V_{PE(drawn)} - V_{PE(undrawn)}]/V_{PE(undrawn)}$.

Herein, we state the predominant factors affecting the **oPs** parameters that must be considered in the interpretation of our results:

(1) The **oPs** do not sample all sites in the polymer with equal probability. In most polymers, including **PE**, the **oPs** prefer to localize in amorphous and interfacial sites, with a preference toward larger sites. As a result, τ_3 will reflect the characteristics (composition, strain state, packing) of the amorphous and interfacial (crystalline-amorphous interphase) portions, and I_3 will reflect both the characteristics of the amorphous and interfacial parts and the amount of the crystalline (less accessible) part in the volume probed. In branched **PE** and copolymers of **PE**, the easily crystallizable and amorphous parts have different compositions, so that the packing and possibly the strain state of the amorphous and interphase regions change as a function of the degree of crystallinity. The I_3 component from the **UHMWPE** films varied with source contact in a manner that did not appear sensitive to the degree of crystallinity.

(2) As mentioned above, the **oPs** formation probability is a function of source contact time for **PE**.

(3) In glassy polymers, the **oPs** are thought to be localized in preexisting nanovoids ("static" free volume) as well as in sites that open and close (dynamic free volume) over periods that can be comparable to the **oPs** lifetimes, depending on the chain mobility. At temperatures far above the glass transition, T_g, the **oPs** tends to see the polymer as a liquid, blowing a bubble around itself and having a lifetime characteristic of the surface tension.[63] In most polymers, including **PE**, this temperature is approximately T_g + 85 °C, and, above this temperature, τ_3 ceases to reflect changes in chain packing and mobility. Hence, room-temperature experiments on samples with T_g < −60 °C must be interpreted with care. That is not a problem with room-temperature measurements on **PE** because its T_g is typically near −30 °C.[64]

Table 2 shows the **oPs** results with **UHMWPE** films at DR = 1−78. There is an initial increase in the mean free volume of "holes" at DR = 1 → 15 that is followed by the expected decrease as the DR is increased above 15[65] (Figure 7). These trends are consistent with the previously discussed changes in crystallinity that occur on drawing and indicate that it affects the amorphous as well as the crystalline regions. During the initial deformation stages, at DR = 1−2, the microfibrils

(55) Greenfield, M. L.; Theodorou, D. N. *Macromolecules* **1993**, *26*, 5461−5472.
(56) Calleja, F. J. B.; Serna, J.; Vicente, J.; Segovia, M. A. *J. Appl. Phys.* **1985**, *58*, 253−259.
(57) Suzuki, T.; Oki, Y.; Numajiri, M.; Miura, T.; Kondo, K.; Ito, Y. *J. Polym. Sci., Polym. Phys.* **1992**, *30*, 517−525.
(58) Ache, H. J. In *Positronium and Muonium Chemistry*; Gould, R. F., Ed.; American Chemical Society: Washington, DC, 1979; Chapter 1.
(59) (a) Brandt, W.; Berko, S.; Walker, W. W. *Phys. Rev.* **1960**, *120*, 1289−1295. (b) Eldrup, M.; Lightbody, M.; Sherwood, J. N. *Chem. Phys.* **1981**, *63*, 51−58.
(60) Tao, S. J. *J. Chem. Phys.* **1972**, *56*, 5499−5510.
(61) Nakanishi, H.; Wang, S. J.; Jean, Y. C. In *Positron Annihilation Studies of Fluids*; Sharma, S. C., Ed.; World Science: Singapore, 1998; p 292.
(62) Hill, A. J. In *Polymer characterization techniques and their application to blends*; Simon, P. S., Ed.; Oxford Press: Washington, 2003; Chapter 14.
(63) Forsyth, M.; Meakin, P.; MacFarlane, D. R.; Hill, A. J. *J. Phys.: Condens. Matter* **1995**, *7*, 7601−7617.
(64) Boyer, R. F. *Macromolecules* **1973**, *6*, 288−299.
(65) The anomalously high, reproducible mean free volume calculated at DR = 52 is not understood at this time.

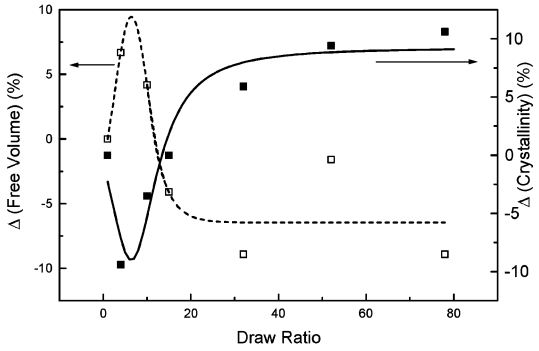

Figure 7. Plots of free volume changes (■) and crystallinity changes (□) of **UHMWPE** films versus their draw ratios. % Δ(free volume) and Δ(crystallinity) are defined in Tables 1 and 2.

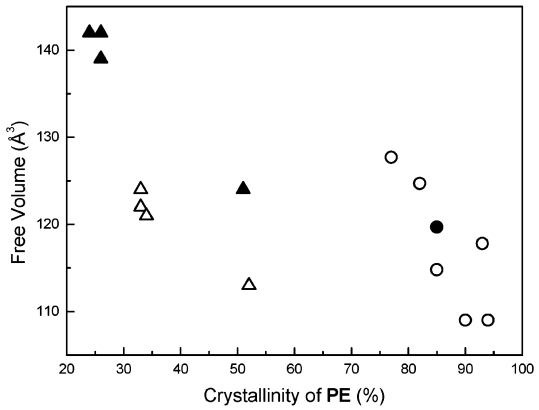

Figure 8. Plots of free volumes (Å^3) of undrawn (●) and drawn (○) **UHMWPE** and other types of undrawn (▲) and drawn (△) **PE**[40a] versus their crystallinities.

undergoing "stretch" and "flip" motions may increase the void volumes of chains around them. The tight packing that occurs as the lamellae unfold at DR > 15 reduces again the void volumes.

The mean free void volumes of undrawn **UHMWPE** are smaller than those of **LDPE** and **HDPE**,[40a] and a highly drawn **UHMWPE** film possesses the smallest void sites of any polyethylene we are aware of (Figure 8). The small mean free volumes in **UHMWPE** should make diffusion of small guest molecules more difficult than in **LDPE** and **HDPE**.[17,28]

Diffusion Studies of DMA in UHMWPE-Py-d Films. Previously, we demonstrated that information about the amorphous region of **UHMWPE** can be obtained from analyses of fluorescence quenching of covalently linked 1-pyrenyl groups by **DMA** in **UHMWPE-Py-g** films.[17] Because of the method of preparation of the **UHMWPE/Py-g** films, the 1-pyrenyl groups are distributed throughout the amorphous regions (i.e., far from film surfaces). For comparison purposes, we have doped pyrene into a **UHMWPE** film by immersing it into a 0.05 M pyrene in chloroform solution for 3 days (yielding **UHMWPE/Py-d**). Pyrene molecules in this and the resulting **UHMWPE-Py-d** films are expected to reside preferentially nearer the film surfaces and be distributed less uniformly than in **UHMWPE/Py-g** and the resulting **UHMWPE-Py-g** films due to hindered diffusion caused by the high crystallinity contents.[36,66] A question that arises is, "Will the different

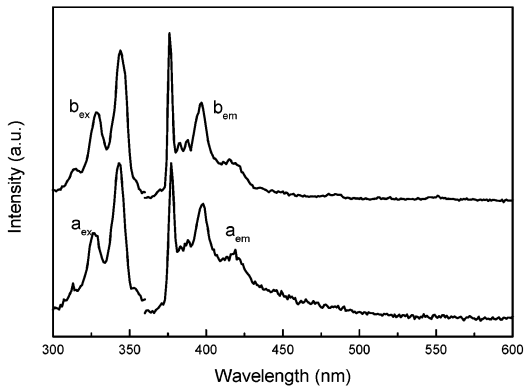

Figure 9. Excitation and emission spectra (λ_{ex} 343 nm and λ_{em} 377 nm) of (a) an undrawn **UHMWPE-Py-d** film after exhaustive extraction with chloroform and (b) an **LDPE** film doped with 10^{-6} mol kg^{-1} of 1-ethylpyrene.

distributions of covalently attached 1-pyrenyl groups in the two films result in different apparent rates of diffusion of **DMA** molecules, as measured from the quenching of pyrenyl fluorescence?" Although the concentration of the attached pyrenyl groups in **UHMWPE-Py-d** was too low to be determined from UV/visible absorption spectra, the similarity of the shapes and peak maxima of its excitation and emission spectra and those of 1-ethylpyrene (Figure 9) indicates that the attachment is primarily at the 1-position of the pyrenyl groups, as expected.[17,28] Fluorescence decay histograms from **UHMWPE-Py-d** can be fitted to an exponential function whose main component (82%) has $\tau = 188$ ns; the minor components are 42.3 ns (15%, probably from an excimeric-like species) and 5.7 ns (3%). These values are virtually the same as those in **UHMWPE-Py-g**.[17]

To perform the **DMA** in-diffusion measurements, undrawn and DR = 10 **UHMWPE-Py-d** films were immobilized on a frame and immersed in a large volume excess of N_2-saturated 0.95 M **DMA**/MeOH solution at constant temperature while the decrease in the intensity of pyrenyl fluorescence was monitored as a function of time (in-diffusion). The films were then immersed in a large volume excess of thermostated neat methanol and the increase of fluorescence intensity was followed (out-diffusion). The time required to reach equilibrium (i.e., the minimum fluorescence intensity and maximum quenching for in-diffusion) in the undrawn and drawn films decreased as temperature was increased, as expected, but there was no discernible temperature dependence on Φ_q (the amount of pyrenyl fluorescence quenched by **DMA** at equilibrium) within the temperature range explored, and the value of Φ_q is virtually the same as that found in the corresponding **UHMWPE-Py-g** films. Because quenching is collisional,[67] and 1-pyrenyl groups must encounter at least one **DMA** molecule during their excited singlet-state lifetimes, these results suggest that the increased mobility and lower concentrations of the **DMA** molecules in the films at higher temperatures may offset each other. In addition, the value of Φ_q in the drawn films is little more than one-half what is found in the undrawn ones. Drawing **UHMWPE** films by even 10-fold "stiffens" significantly the walls of the sites[68] in which the 1-pyrenyl groups reside and, from

(66) (a) Konwerska-Hrabowska, J.; Chantry, G. W.; Nicol, E. A. *Int. J. Infrared Millimeter Waves* **1981**, *2*, 1135−1149. (b) Jang, Y. T.; Phillips, P. J.; Thulstrup, E. W. *Chem. Phys. Lett.* **1982**, *93*, 66−79.

(67) Lakowicz, J. R. *Principles of Fluorescence Spectroscopy*; Kluwer Academic: New York, 1999; p 11.

(68) Weiss, R. G.; Ramamurthy, V.; Hammond, G. S. *Acc. Chem. Res.* **1993**, *26*, 530−536.

Table 3. Diffusion Coefficients (D, $cm^2\ s^{-1}$) and Other Parameters for **DMA** Diffusion within Undrawn **UHMWPE-Py-d** and **UHMWPE-Py-g** Films[17] [a]

			in-diffusion			out-diffusion		
film type	T (°C)	Φ_q (%)[b]	α_{in}	$10^{10}D_{in1}$	$10^{9}D_{in2}$	α_{out}	$10^{10}D_{out1}$	$10^{9}D_{out2}$
UHMWPE-Py-d	15.3	40	0.72 ± 0.02	1.4 ± 0.2	3.5 ± 0.1	0.76 ± 0.02	4.0 ± 0.2	1.3 ± 0.5
	26.4	38	0.70 ± 0.01	6.3 ± 0.8	17 ± 2.1	0.71 ± 0.02	8.1 ± 0.2	7.9 ± 0.4
	34.1	44	0.53 ± 0.03	58 ± 2.3	58 ± 5.1	0.60 ± 0.04	37.0 ± 2.1	12.0 ± 1.4
	44.5	40	0.40 ± 0.02	160 ± 50	147 ± 15	0.46 ± 0.05	180 ± 5.1	50.0 ± 2.7
	52.3	35	0.32 ± 0.01	420 ± 40	350 ± 26	0.39 ± 0.03	340 ± 12	80.0 ± 9.1
UHMWPE-Py-g	15.7	39	0.33 ± 0.04	1.05 ± 0.07	0.95 ± 0.11	0.51± 0.04	0.99 ± 0.37	2.01 ± 0.90
	24.7	37	0.27 ± 0.02	2.86 ± 0.37	2.47 ± 0.15	0.47 ± 0.17	4.23 ± 1.61	4.09 ± 2.53
	35.3	40	0.32 ± 0.08	18.0 ± 6.3	8.03 ± 3.20	0.29 ± 0.06	8.75 ± 4.56	7.02 ± 2.50
	45.0	42	0.20 ± 0.08	27.6 ± 5.2	24.8 ± 5.70	0.45 ± 0.19	36.7 ± 7.3	34.2 ± 9.4
	49.5	36	0.17 ± 0.08	41.6 ± 10.1	46.2 ± 8.1	0.36 ± 0.20	53.0 ± 12.1	51.3 ± 9.0

[a] For in-diffusion, the films were immersed in 0.95 M **DMA** in methanol solutions. For out-diffusion, the films were immersed in neat methanol. [b] $\Phi_q = 1 - I_\infty/I_0(\pm 1.5\%)$, in which I_0 and I_∞ refer to the fluorescence intensities (λ_{ex}: 343 nm; λ_{em}: 377 nm) at the time = 0 and "∞" (i.e., at equilibrium), respectively.

Table 4. Diffusion Coefficients (D, $cm^2\ s^{-1}$) and Other Parameters for **DMA** Diffusion within DR = 10 **UHMWPE-Py-d** and DR = 9 **UHMWPE-Py-g** Films[17] [a]

			in-diffusion			out-diffusion		
film type	T (°C)	Φ_q (%)[b]	α_{in}	$10^{11}D_{in1}$	$10^{10}D_{in2}$	α_{out}	$10^{11}D_{out1}$	$10^{9}D_{out2}$
UHMWPE-Py-d (DR = 10)	15.4	24	0.89 ± 0.02	3.5 ± 0.5	5.2 ± 0.9	0.90 ± 0.02	3.1 ± 0.6	4.3 ± 0.6
	25.7	23	0.75 ± 0.01	13.0 ± 1.7	20 ± 3.4	0.72 ± 0.02	12.0 ± 1.9	9.8 ± 1.3
	35.8	27	0.32 ± 0.03	110 ± 17.1	120 ± 15.3	0.72 ± 0.02	81.1 ± 10.6	54.4 ± 6.7
UHMWPE-Py-g (DR = 9)	17.4	20	0.53 ± 0.15	0.10 ± 0.04	0.16 ± 0.04	0.49 ± 0.17	0.17 ± 0.02	2.38 ± 0.37
	24.0	19	0.39 ± 0.09	0.22 ± 0.10	0.35 ± 0.10	0.46 ± 0.15	0.35 ± 0.06	4.55 ± 0.95
	34.9	25	0.31 ± 0.08	8.02 ± 3.02	6.56 ± 2.38	0.46 ± 0.11	10.5 ± 2.89	9.23 ± 2.21

[a] For in-diffusion, the films were immersed in 0.95 M **DMA** in methanol solutions. For out-diffusion, the films were immersed in neat methanol. [b] ±1.7%.

the diffusion coefficients (D; see below), makes access to them by **DMA** molecules more difficult.

At any time t, C_t/C_0, the fraction of pyrenyl groups with at least one **DMA** molecule as a neighbor within a film, should be equal to the fraction of pyrenyl excited singlet states that are quenched by **DMA**. In terms of fluorescence intensities, $C_t/C_0 = (I_t - I_\infty)/(I_0 - I_\infty)$, where I_t is the fluorescence intensity at time = t, I_0 is obtained from the intercept of the slope of the linear region of a plot of fluorescence intensity versus $t^{1/2}$,[29a,69] and I_∞ is the intensity after long times when its value no longer changes perceptibly. In this way, the fluorescence data for in- and out-diffusion of **DMA** can be treated according to integrated forms of Fick's second law, eqs 2 and 3,[17,70] respectively, in which l is the film thickness (cm) and D has units of $cm^2\ s^{-1}$.

As with **UHMWPE-Py-g** films, two diffusion coefficients, D_1 and D_2, are required to fit well the **DMA** diffusion data in **UHMWPE-Py-d** films; α is the fraction of diffusion occurring via the D_1 process. The best fit was achieved by adjusting the value of α empirically so that the difference, $\sum|I_t - I_t^{fit}|^2$, was minimized.

$$\frac{I_t - I_\infty}{I_0 - I_\infty} = \alpha\frac{8}{\pi^2}\sum_{n=0}^{15}\frac{1}{(2n+1)^2}e^{-D_1(2n+1)^2\pi^2 t/l^2} + (1-\alpha)\frac{8}{\pi^2}\sum_{n=0}^{15}\frac{1}{(2n+1)^2}e^{-D_2(2n+1)^2\pi^2 t/l^2} \quad (2)$$

$$\frac{I_t - I_\infty}{I_0 - I_\infty} = 1 - \alpha\frac{8}{\pi^2}\sum_{n=0}^{15}\frac{1}{(2n+1)^2}e^{-D_1(2n+1)^2\pi^2 t/l^2} - (1-\alpha)\frac{8}{\pi^2}\sum_{n=0}^{15}\frac{1}{(2n+1)^2}e^{-D_2(2n+1)^2\pi^2 t/l^2} \quad (3)$$

The magnitudes of the diffusion coefficients, $(D_{in})_i$ and $(D_{out})_i$, for in- and out-diffusion of **DMA** in undrawn and DR = 10 **UHMWPE-Py-d** films increase with increasing temperature, while, qualitatively, the values of α decrease (Tables 3 and 4). Because of the nature of our experimental apparatus, the first tens of seconds of diffusion data are not recorded. As a result, the importance of the faster diffusion components, D_2, is underestimated, and the reported α values are overestimates. Despite these limitations, the decreases in α from increasing temperature during in-diffusion are clearly much larger than those during out-diffusion, and the absolute magnitudes of the D values (that are not affected by the imprecision in α) indicate significantly increased resistance to **DMA** movement upon drawing both **UHMWPE-Py-d** and **UHMWPE-Py-g** films.

On the basis of the larger mean free volumes of DR = 10 **UHMWPE** (Table 2 and Figure 7), **DMA** molecules are predicted to move more rapidly within it than in undrawn **UHMWPE**. However, just the opposite relationship is found in both **UHMWPE-Py-d** and **UHMWPE-Py-g** films. Other factors that control the movement of diffusing molecules from site to site, such as wall stiffness,[68] must be more important than the mean free volume.

Although the Φ_q values indicate similar distributions of attached 1-pyrenyl groups in **UHMWPE-Py-d** and **UHMWPE-Py-g** films, the larger diffusion coefficients in the **UHMWPE-Py-d** films suggest that the pyrenyl groups in **UHMWPE-Py-g**

(69) Crank, J. *The Mathematics of Diffusion*; Oxford: London, 1956; p 45.
(70) Comyn, J. *Polymer Permeability*; Elsevier: London, 1985; Chapter 1.

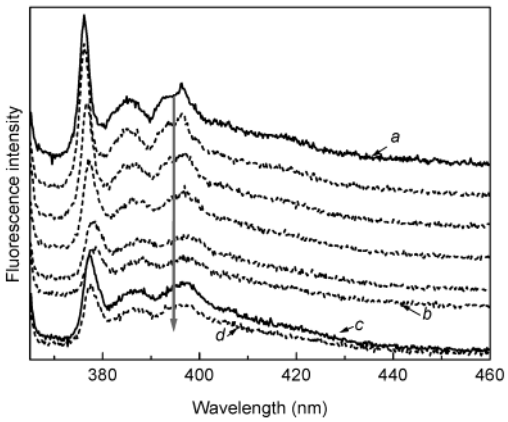

Figure 10. Selected emission spectra (λ_{ex} 343 nm) of an undrawn **UHMWPE-Py-g** film at different temperatures. The vertical arrow indicates the direction of temperature increase from −233 (a) to 127 °C (b). Spectra c and d were recorded at room temperature before and after, respectively, the cooling and heating protocol. The curves are offset from each other on the vertical axis for clarity.

Table 5. Activation Energies (E, kJ mol^{-1}) for **DMA** Diffusion in **UHMWPE-Py-d** Films

DR	E_{in1}	E_{in2}	E_{out1}	E_{out2}
1	124 ± 18	97 ± 10	101 ± 14	87 ± 11
10	130 ± 20	119 ± 14	124 ± 16	106 ± 17

films are located, on average, in less accessible amorphous regions (i.e., that may be surrounded by more crystalline regions or be more ordered[66]).

The activation energies for **DMA** diffusion in **UHMWPE-Py-d** can be obtained from Arrhenius-type plots and the diffusion coefficients in Tables 3 and 4 (Table 5 and Figures 1 and 2 of Supporting Information). The activation energies in the undrawn film are similar to those in **UHMWPE-Py-g**.[17] From this, we infer that the environments provided to that fraction of attached pyrenyl groups that can be quenched by **DMA** molecules are similar in the films of **UHMWPE-Py-d** and **UHMWPE-Py-g**. Because of the number of data points employed in the calculations and the temperature ranges over which the data were collected, the activation energies in the drawn films are inherently less accurate than those in the undrawn ones. Despite the fact that the large error limits (and small temperature range for data from the drawn film) bring the E values from the undrawn and DR = 10 film within the same range, the average values from the drawn film tend to be somewhat larger than those from the undrawn one. It should be remembered that the diffusion data and the activation energies from which they are derived are based on only ca. 40% of the pyrenyl groups in the undrawn **UHMWPE-Py-d** film and ca. 25% in the drawn one; we derive no information from these studies about the sites in which the other (unquenched) pyrenyl groups reside.

Fluorescence Spectra of Undrawn and DR = 9 and 48 UHMWPE-Py-g Films at Different Temperatures. Figure 10 shows emission spectra of an undrawn **UHMWPE-Py-g** film as a function of temperature. The intensities are directly comparable because neither the instrument parameters nor the position of the film was changed during a set of runs. As expected, the intensity of the emission at the lowest temperature investigated, −233 °C (spectrum a), is much higher than that of the spectrum recorded at room temperature (room temperature, spectrum c). The lower intensity of the spectrum after the film was heated to 127 °C (i.e., near its melting temperature, ca. 129 °C,[17] spectrum b) and recooled to room temperature (spectrum d) is consistent with the morphology changes detected during the DSC experiments (Figure 6).

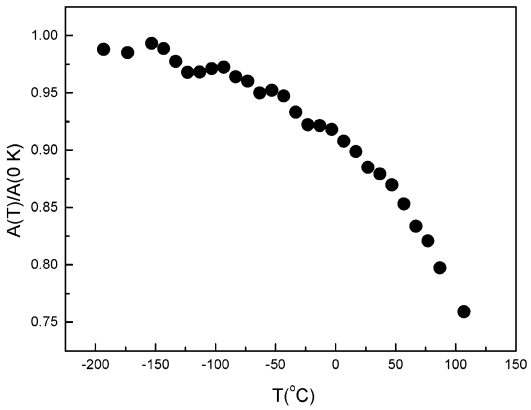

Figure 11. Emission area (369−460 nm) ratios of data from Figure 9 versus temperature. See text for details.

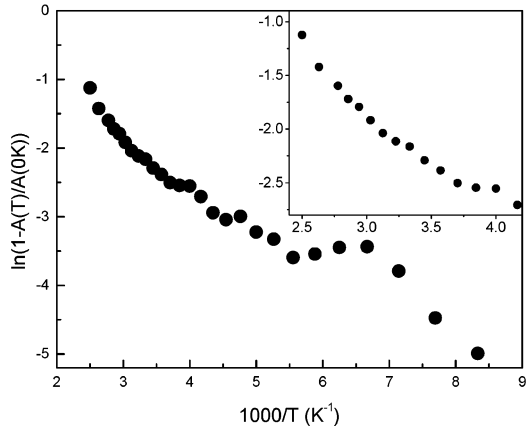

Figure 12. Arrhenius-type plot of the data in Figure 11. The inset expands data points in the high-temperature region.

Normalized integrated fluorescence intensities (as total areas between 369 and 460 nm) versus temperature for the data in Figure 10 are plotted in Figure 11. An Arrhenius-like treatment of the same data according to eq 4 is shown in Figure 12. A_{pre} is the preexponential term, and E_a is the associated activation energy; $A(T)$ and $A(0)$ are the integrated fluorescence intensities at temperature = T and are extrapolated to the limiting value at 0 K. $A(0)$ has been taken as the average of the intensities in the low-temperature plateau region, from −193 to −143 °C. The invariance of the position of the maximum intensity of the blue-edge emission peak in this temperature region is another indicator that the data approximate the "0 K" value (vide infra; Figure 14).

$$\ln(1 - A(T)/A(0)) = A_{pre} - E_a/RT \qquad (4)$$

Two small excursion regions in the inset of Figure 12 are seen in the ca. 40−80 °C and − 25 to −15 °C temperature ranges. They occur where α- and β-relaxations, respectively, have been reported for other types of **PE**.[18,30] The α-relaxation process has been attributed to changes in the amorphous regions in polyethylenes that have crystalline regions nearby,[30b] and β-processes have been ascribed to the glass−rubber relaxations

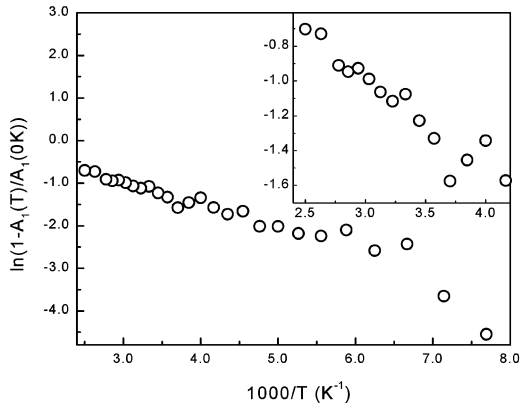

Figure 13. Arrhenius-type plots of the area under the deconvoluted blue-edge emission peak (A_1) of an undrawn **UHMWPE-Py-g** film versus temperature. The inset expands data points in the high-temperature region.

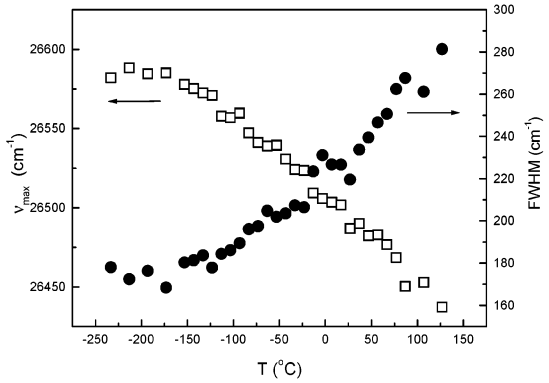

Figure 14. The fwhm (●) and wavenumber at maximum intensity of the deconvoluted blue-edge emission peak (□) versus temperature of an undrawn **UHMWPE-Py-g** film.

of the amorphous fractions.[30] To separate and measure the area under the blue-edge emission peak (from the 0−0 band[35]), the spectrum was deconvoluted into Gaussian components.[49] The neat area under the blue-edge emission peak (intensity max at λ_{em} = 377 nm) and its full peak-width at half-height (fwhm) were then obtained. The resulting data are also plotted in an Arrhenius-like fashion using eq 4 (Figures 13 and 14). The two excursion regions in the ca. 40−80 °C and − 25 to −15 °C temperature ranges noted above are more pronounced here. The invariance of both the fwhm and the frequency maximum of the blue-edge emission peak below ca. −120 °C is consistent with the polyethylene chains being essentially immobile in this temperature range.

The corresponding Arrhenius-type (A) and fwhm (B) plots of fluorescence data from DR = 9 and 48 **UHMWPE-Py-g** films were also examined (Figure 15). The two excursion regions detected from the undrawn film persist up to DR = 48. These results are similar to those reported previously using fluorescence from anthracene molecules or covalently attached 9-anthryl groups in **LDPE** films.[30c] They are also consistent with the data from PALS that significant free volume remains in highly drawn **UHMWPE**. The slope changes in Arrhenius plots for **UHMWPE** (Figures 12, 13, and 15) are much smaller than those in **LDPE**.[30c] We suggest that the stiffer chains in **UHMWPE** are less able than **LDPE** to couple with the excited states of nearby 1-pyrenyl groups.[71] As a result, the sensitivity of the reporter groups is attenuated.

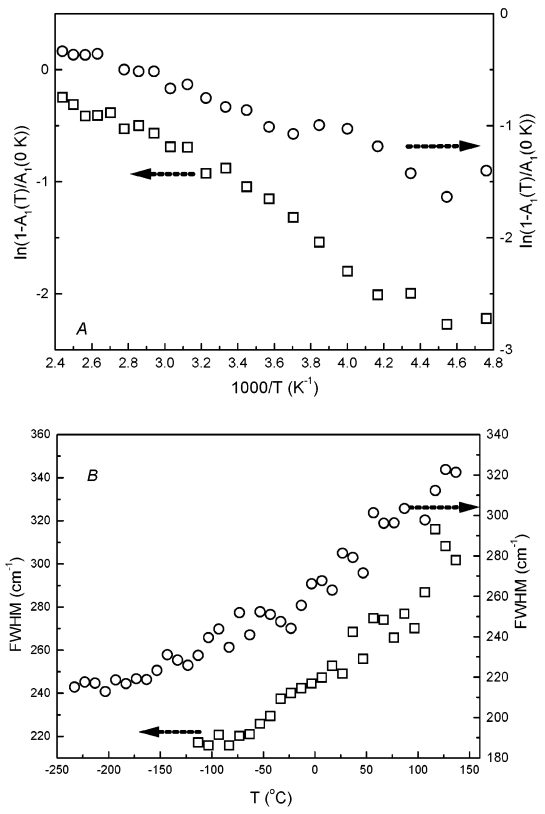

Figure 15. Arrhenius-type plots of the area ratios under the blue-edge emission peaks (A) and the temperature dependence of their fwhm (B) for DR = 9 (□) and 48 (○) **UHMWPE-Py-g** films.

Polarized Absorption and Emission Spectra of Drawn UHMWPE/Py Films. Drawn polyethylene films are commonly used to orient aromatic molecules[72,73] or dichroic dyes,[74] and the degree of orientation, as provided by the orientation factor, K_z,[75] can supply important information concerning the sites where the guests reside.[17,36] In **LDPE** films, the magnitudes of linear dichroic parameters increase with decreasing temperature and plateau near −20 °C.[76]

Polarized Absorption Spectra. From plots of the temperature dependence on fluorescence parameters provided above, the onset of the β-relaxation process (or glass transition[3]) for the undrawn and drawn **UHMWPE** films occurs between −25 and −15 °C. Dichroic measurements on DR = 9 **UHMWPE/Py-g** and DR = 10 **UHMWPE/Py-d** films have been conducted at −25 and −30 °C to ensure limiting values. Both sets of measurements indicate that the **UHMWPE** matrix is very stiff even at room temperature because the values of K_z at temperatures between −25 and −30 °C (0.46 ± 0.02 (**g**) and 0.48 ± 0.02 (**d**)) and at room temperature (0.44 ± 0.02 (**g**) and 0.46 ± 0.03 (**d**)) are very similar. In addition, the similarity between the degrees of polarization of pyrene molecules in drawn **UHMWPE/Py-d** and **UHMWPE/Py-g** films is consistent with the conclusions derived from the **DMA** quenching experiments

(71) Schurr, O.; Yamaki, S. B.; Wang, C.; Atvars, T. D. Z.; Weiss, R. G. *Macromolecules* **2003**, *36*, 3485−3497.
(72) Thulstrup, E. W.; Michl, J. *J. Phys. Chem.* **1980**, *84*, 82−93.
(73) Konwerska-Hrabowska, J. *Appl. Spectrosc.* **1985**, *39*, 976−979.
(74) Tirelli, N.; Amabile, S.; Cellai, C.; Pucci, A.; Regoli, L.; Ruggeri, G.; Ciardelli, F. *Macromolecules* **2001**, *34*, 2129−2137.
(75) $K_z = D_z/(D_z + 2)$, where the dichroic ratio $D_z = (OD)_{z,||}/(OD)_{z,\perp}$, and $OD_{||}$ and $OD_\perp$ are the polarized absorbances at a specific wavelength.[72]
(76) Steenstrup, F. R.; Christensen, K.; Svane, C.; Thulstrup, E. W. *J. Mol. Struct.* **1997**, *408*, 139−148.

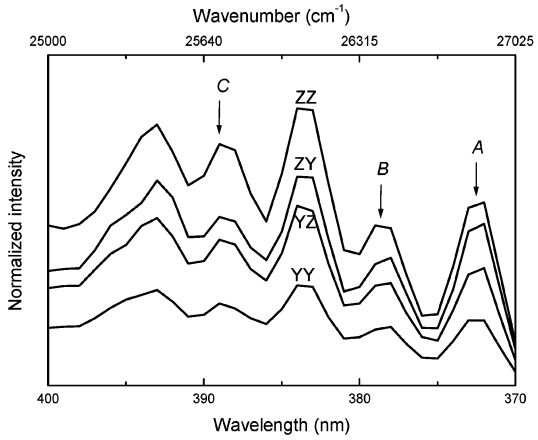

Figure 16. Corrected polarized emission spectra of 2.8×10^{-3} mol kg^{-1} of pyrene in a DR = 9 **UHMWPE-Py-g** film at −45 °C (λ_{ex} 336 nm, ^1L_a-origin;[35] the band-pass is 4.5 and 1.8 nm for excitation and emission, respectively). See text for details.

Scheme 1. Pyrene Axes Designations

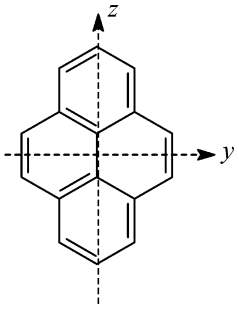

that the two modes of introducing pyrene into the films lead to similar site distributions.

Polarized Emission Spectra. Polarized emission spectra were recorded between room temperature and − 45 °C. Instrumental correction factors[35] (from the polarized emission spectra of a solution of 1.0×10^{-4} M pyrene in N_2-saturated hexanes at room temperature that are assumed to be completely depolarized) and baseline corrections (by extrapolation of the backgrounds at 550−600 nm to lower wavelengths) were employed during the analyses. The intensity of the *YZ* and *ZY* orientations (where *Y* and *Z* refer to electric vectors of polarized light at horizontal and vertical positions, respectively, and the first and second letters refer to the incident and the emitted light, respectively) was ratioed to that at the *ZZ* position (Figure 3 of Supporting Information).

Figure 16 shows the four corrected polarized emission spectra from pyrene molecules in the **UHMWPE/Py-g** film with DR = 9 at −45 °C. The (A) emission peak has been identified as purely *y*-polarized, and the 336 nm excitation band has been identified as purely *z*-polarized (where the *z* and *y* are the long and short molecular axes, respectively, of pyrene; Scheme 1).[77] For a purely polarized absorption (along the *z* molecular axis) and emission (along the *y* molecular axis), the relative intensities $I_{ZY(zy)}$ of the polarized fluorescence are proportional to the tensor elements $S_{ZY(zy)}$.

The *z*-polarized contribution to the mixed *y*- and *z*-polarized peaks, (B) and (C), have been determined by a stepwise reduction procedure.[78] The ratio of the tensor elements, $S_{UV}(uv)$ and $S_{ST}(uv)$, where *S*, *T*, *U*, and *V* can be *X*, *Y*, or *Z*, is obtained by finding the linear combinations of I_{UV} and I_{ST} intensities in which the *uv*-polarized spectral feature (where *u* and *v* refer to molecular axes *x*, *y*, and *z*; Scheme 1) disappears (i.e., $I_{UV} - [S_{UV}(uv)/S_{ST}(uv)]I_{ST} = 0$).[35]

$$S_{ZZ}(uv):S_{YZ}(uv):S_{ZY}(uv) = L_{uv}:[(K_v - L_{uv})/2]:[(K_u - L_{uv})/2] \quad (5)$$

The ratios of the tensor elements $S_{UV}(uv)$ are related to the orientation factors, K_u and L_{uv}, according to eq 5.[35,77] K_u and K_v are linear dichroic parameters obtained from the linearly polarized absorption spectra (vide ante). The fourth moment L_z (or L_{zz}) values have been calculated from eq 5 and the relative intensities of polarized fluorescence in Table 6. As temperature is varied, so are the orientations of guest molecules in **LDPE** as the rates of motion of polymer chains, and, thereby, the rates of guest molecule translations and rotations are changed. Reducing temperature increases the specificity of orientation.[76,79] In **UHMWPE**, the invariance of the orientation factors (within the limits of experimental error), K_u and L_{uv}, to temperature over the range explored implies again that the polyethylene chains near the reporter groups are very stiff even at room temperature. Pyrene molecules are predicted to have limited mobility based on volume considerations as well: the van der Waals volume of a pyrene molecule is estimated to be ca. 322 Å^3,[80] while the mean void volumes of "holes" in native **UHMWPE** are calculated to be only ca. 110−130 Å^3 (Table 2).

The relationship between K_z^2 and L_z is an indicator of the distribution of molecular orientations. The closer are the values of K_z^2 and L_z, the closer to parallel are the *z*-axis of pyrene molecules and the axis of draw (set parallel to the *Z*-axis in our experiments):[35] $K_z^2 = 0.21 \pm 0.01$ at temperatures between −25 and −30 °C and $L_z = 0.23 \pm 0.01$ at −29 °C. We consider this an excellent match and conclude that (1) the fraction of pyrene molecules whose orientation deviates substantially from the mean must be very small and (2) the distribution of orientations is unimodal.

Table 6. The Ratios of the Tensor Elements, $S_{ZZ}(uv)/S_{ZY}(uv)$ and $S_{ZZ}(uv)/S_{YZ}(uv)$, and the Fourth Moment, L_z, of Fluorescence Polarizations from a DR = 9 **UHMWPE/Py-g** Film at Different Temperatures[a]

T (°C)	*u*	*v*	$S_{ZZ}(uv)/S_{ZY}(uv)$	$S_{ZZ}(uv)/S_{YZ}(uv)$	L_z
room temp	*z*	*y* (α)	1.36 ± 0.03	1.97 ± 0.04	0.19 ± 0.02
	z	*z* (β,γ)	1.46 ± 0.09	1.86 ± 0.01	
−2	*z*	*y* (α)	1.66 ± 0.03	1.31 ± 0.05	0.19 ± 0.02
	z	*z* (β,γ)	1.90 ± 0.10	1.25 ± 0.01	
−15	*z*	*y* (α)	1.44 ± 0.08	1.80 ± 0.04	0.21 ± 0.01
	z	*z* (β,γ)	1.65 ± 0.10	1.79 ± 0.01	
−29	*z*	*y* (α)	1.49 ± 0.05	1.91 ± 0.07	0.23 ± 0.01
	z	*z* (β,γ)	2.06 ± 0.08	2.03 ± 0.08	
−45	*z*	*y* (α)	1.20 ± 0.02	1.60 ± 0.03	0.19 ± 0.02
	z	*z* (β,γ)	1.46 ± 0.06	1.59 ± 0.03	
	z	*z* (β,γ)	1.51 ± 0.12	1.55 ± 0.06	

[a] The data are based on relative fluorescence intensities of pyrene in the *y* and *z* directions as calculated from different emission bands; see text for details.

(77) Langkilde, F. W.; Gisin, M.; Thulstrup, E. W.; Michl, J. *J. Phys. Chem.* **1983**, *87*, 2901−2911.
(78) Michl, J.; Thulstrup, E. W. *J. Chem. Phys.* **1980**, *72*, 3999−4008.
(79) Wang, C.; Xu, J.; Weiss, R. G. *J. Phys. Chem. B* **2003**, *107*, 7015−7025.
(80) Camerman, A.; Trotter, J. *Acta Crystallogr.* **1965**, *18*, 636−643.

Conclusions

Even in the undrawn state of gel-crystallized **UHMWPE** films, polyethylene chains are arranged somewhat anisotropically. As strain is applied initially, preformed microfibrils are deformed during "stretch" and "flip" motions that depend on their initial orientations with respect to the draw direction. In addition, the initial deformations (DR < 15) cause morphological changes in both the crystal and the amorphous regions that are manifested as decreases in the degree of crystallinity and increases in the mean free void volumes. At draw ratios greater than 15, lamellae of the microfibrils fold, allowing more tightly packed extended chains, increased crystallinity, and decreased mean free void volumes. Besides the dominant orthorhombic phase, small amounts of monoclinic and triclinic crystals were observed in the drawn films. They are the probable source of the small endotherm observed at temperatures lower than the orthorhombic melting in DSC thermograms of **UHMWPE** at $1 < DR < 15$.

Because of the high crystalline content of **UHMWPE**, its amorphous chains are stiffer than those of other types of **PE**. Results in films at different draw ratios indicate that changes in chain stiffness are a more important factor than changes in mean free volumes in mediating diffusion of a small guest molecule, **DMA**, within the amorphous regions of **UHMWPE**. Those studies were made possible by the attachment of 1-pyrenyl groups to the polyethylene chains using a photochemical labeling procedure. The stiff microstructures within the amorphous regions also reduce the ability of the excited singlet states of the noncovalently attached reporter molecule, pyrene, to sense the onsets of α- and β-relaxation processes that occur nearby, and make its orientation factors almost insensitive to temperature in the range investigated.

These results present a rather comprehensive picture of the static and dynamic properties of **UHMWPE** films at various degrees of draw. As such, they should be useful in understanding "creep", a property deleterious to commercial applications of **UHMWPE**.[9]

Acknowledgment. The Georgetown group is grateful to the National Science Foundation for financial support. Drs. Gerald O. Brown and Oliver Schurr are thanked for technical assistance. Dr. Ivan Chodak is thanked for several useful suggestions and criticisms. We also thank Dr. Travis Holman for valuable discussions on the X-ray diffraction experiments. This paper is dedicated to six eminent photochemists, Robert S. H. Liu, Douglas C. Neckers, Jack Saltiel, Nicholas J. Turro, Peter J. Wagner, and David G. Whitten, who celebrate their 65th birthdays during 2003.

Supporting Information Available: Three figures: Arrhenius-type plots of D_{in} and D_{out} for **DMA** diffusion in undrawn and DR = 10 **UHMWPE-Py-d** films, and the ratios of intensities of polarized emission spectra from 10^{-4} M pyrene in nitrogen-saturated hexane (PDF). This material is available free of charge via the Internet at http://pubs.acs.org.

JA0362205